Biological Trace Element Research (2020) 193:282–293
https://doi.org/10.1007/s12011-019-01700-y

Synthesis and Biodistribution Study of Biocompatible ^{198}Au Nanoparticles by use of Arabinoxylan as Reducing and Stabilizing Agent

Fozia Iram[1] · Mohammad S. Iqbal[2] · Irfan U. Khan[3] · Rashid Rasheed[4] · Aqsa Khalid[1] · Muhammad Khalid[5] · Saira Aftab[6] · Abdul R. Shakoori[6]

Received: 2 January 2019 / Accepted: 18 March 2019 / Published online: 29 March 2019

Abstract

Radioactive gold-198 is a useful diagnostic and therapeutic agent. Gold in the form of nanoparticles possesses even more exciting properties. This work aimed at arabinoxylan-mediated synthesis and biodistribution study of radioactive gold nanoparticles (^{198}AuNPs). The particles were synthesized by mixing suspension of arabinoxylan with $H^{198}AuCl_4$ without use of any additional reducing and stabilizing agents. An aqueous suspension of arabinoxylan was added to a $H^{198}AuCl_4$ solution, which resulted in reduction of Au^{3+} to ^{198}AuNPs. Biodistribution was studied in vitro and in rabbit. The particles having exceptional stability were readily formed. Highest radioactivity was recorded in spleen after 3 h followed by liver, heart, kidney, and lungs after *i.v.* administration. After 24 h, the activity was not detectable in the spleen; it accumulated in the liver. However, after oral administration, the activity mainly accumulated in the colon. In serum proteins, the distribution was α_1-globulin 6.5%, α_2-globulin ~2%, β-globulin ~1%, γ-globulin 0.7%, and albumin 0.7% of the administered dose. This indicates a low protein binding implying high bioavailability of the particles. The cytotoxicity study showed that the particles were inactive against HeLa cell line and *Agrobacterium tumefaciens*. Highly stable ^{198}AuNPs reported in this work have the potential for targeting the colon. They show affinity for globulins, the property that can be used in the study of the immune system.

Keywords Hemicelluloses · Arabinoxylan · Gold nanoparticles · Targeted delivery · Radioactive gold nanoparticles

Introduction

AuNPs are being widely studied for their potential applications in therapy, diagnosis, drug delivery, and imaging due to their unique properties such as inertness, ease of synthesis, functionalizability, and peculiar optical properties [1–8]. The efficiency of NPs in biomedical imaging largely depends on their optical properties. The size-dependent optical properties of AuNPs, including linear surface plasmon resonance, fluorescence, and Raman scattering, make them ideal candidate for organ imaging and optical sensors [9–11]. The particles having size 3–40 nm absorb at 510–530 nm with extinction coefficients to the order of 10^{11} mol^{-1} cm^{-1} that is much higher than those of conventional dyes used for imaging. In case of particles > 40 nm, the scattering-to-absorption ratio is several orders higher than those of fluorescent dyes [12, 13]. On account of these properties, AuNPs have been widely investigated for diagnostic imaging [4, 14]. AuNPs have also been investigated for their use in photothermal destruction of cancerous cells due to their excellent thermal conductivity [1, 15, 16].

In the present work, we hypothesize that AuNPs encapsulated in arabinoxylan (AX), a swellable hemicellulosic

✉ Mohammad S. Iqbal
saeediq50@hotmail.com

[1] Department of Chemistry, LCW University, Lahore 54600, Pakistan

[2] Department of Chemistry, Forman Christian College, Lahore 54600, Pakistan

[3] Radiopharmacy & PET Radiochemistry Division, Institute of Nuclear Medicine and Oncology, Lahore, Pakistan

[4] Institute of Nuclear Medicine Oncology and Radiotherapy, Abbottabad, Pakistan

[5] Isotope Production Division, Pakistan Institute of Nuclear Science and Technology PO Nilore, Islamabad, Pakistan

[6] School of Biological Sciences, University of the Punjab, Quaid-e-Azam Campus, Lahore 54590, Pakistan

material, would exhibit organ-specific uptake, and if the gold is radioactive, they can be used for radioimaging. ^{198}Au is a radioactive isotope of gold that emits β-particles and γ-rays of energies 0.412, 0.68, and 1.09 MeV. The γ-radiation of 0.412 MeV energy is highly suitable for imaging human organs. On the other hand, β-particles have been successfully employed for treating prostate tumors [17–25].

Generally, AuNPs are synthesized by chemical methods involving use of highly toxic reducing agents such as sodium borohydride, hydrazine, or formaldehyde [26–28] and capped with stabilizing agents, although the particles are thoroughly washed but the process does not rule out the presence of residual amount of the toxic reducing agents. For biomedical applications, the particles need to be absolutely free from toxic materials. In order to ensure this, the use of toxic materials in the synthesis of NPs has to be eliminated. Recently, highly biocompatible and biodegradable materials have been identified as reducing and stabilizing agents. These include hemicelluloses, which can simultaneously reduce Au^{3+} to Au^0 and stabilize them for more than 3 years [29, 30].

In the present study, we have used AX from ispaghula (*Plantago ovata*) husk for the synthesis and stabilization of radioactive ^{198}AuNPs coupled with their biodistribution in vitro and in vivo. AX has the potential to deliver encapsulated drugs at colon as this material is insoluble in acidic and soluble in alkaline media [31]. Thus, when administered orally, the AX-encapsulated AuNPs are expected to remain intact in the stomach (pH < 2) and pass onto the intestine where they get dissolved and hydrolyzed due to alkaline pH and the presence of micro flora there [32]. They are not digested in the small intestine and can easily pass to the colon where they can be partially digested and release encapsulated particles. Moreover, the hydrophilic nature of AX and its high affinity towards mucosal surfaces would assist the encapsulated particles to be released for longer periods of time at the specific site [33]. Thus, we hypothesize that AX-encapsulated ^{198}AuNPs are biocompatible and suitable for diagnosis and therapy of colon-related malignancies.

Materials and Methods

Materials

The materials used in this study were gold (ARY Gold, Lahore, 99.99%), NaOH, HNO_3, and HCl, Extrapure® from E. Merck, Germany; L-(+)-arabinose, D-(+)-galactose, D-glucose, D-(+)-xylose, L-rhamnose monohydrate, galacturonic acid, and citric acid from E. Merck, Germany; oligosaccharides β-(1-4)-D-xylotriose, β-(1-4)-D-xylotetraose, β-(1-4)-D-xylopentaose, and β-(1-4)-D-xylohexaose used as GPC standards were from Megazyme (Sydney, Australia); reactant-free AuNPs (30 nm) stabilized in phosphate buffer, Coomassie Brilliant Blue R-250, dimethyl sulfoxide (DMSO), glycerol, bovine serum albumin (BSA), human serum albumin (HSA), neutral red, glacial acetic acid, *l*-cysteine, disodium hydrogen phosphate, sodium nitrate, and sodium dodecyl sulfate (SDS) were of analytical grade from Sigma Aldrich (USA); *A. tumefaciens*, HeLa cells (ATCC: CCL 2) from Flow Labs (London, UK); Dulbecco's Modified Eagle Medium (DMEM), fetal bovine serum (FBS) from Gibco (USA); complement protein C_3 kit was from Orion Diagnostica (Finland). AX (molar mass 3.17×10^6 Da) was a gift from Dr. Shazma Massey of FC College, Lahore, isolated according to the reported method [34]. The AX sample was recharacterized by elemental analysis, monosaccharide composition, ATR-FT-IR, and gel permeation chromatography (GPC). Nanopure® water was used throughout this work. All the chemicals were used without further purification.

Preparation of $H^{198}AuCl_4 \cdot 3H_2O$

The gold foil (0.050 g) was irradiated with a neutron flux of 8×10^{13} n·cm^{-2}·s^{-1} for 30 min at the research reactor of Pakistan Institute of Nuclear Science and Technology, Islamabad. The irradiated gold was dissolved in aqua regia (150 μL) at 100 °C, evaporated near to dryness, followed by addition of HCl (0.01 M) and evaporation near to dryness. The evaporation process was repeated three times and the remaining mass was left at room temperature for crystallization of $H^{198}AuCl_4 \cdot 3H_2O$.

Synthesis of ^{198}AuNPs

The ^{198}AuNPs were synthesized as reported earlier for non-radioactive AuNPs [29]. Briefly, $H^{198}AuCl_4 \cdot 3H_2O$ (0.0393 g, 0.1 mmol) was dissolved in water (100 mL); to 20 mL of this solution, 20 mL of AX suspension (0.1% in water) was added under vigorous stirring for 2 h at 50 °C. A successive change in color from pale yellow to red was observed in 25 min, indicating the formation of ^{198}AuNPs; however, the stirring was continued for further 2 h to ensure complete reduction. The particles were isolated by centrifugation at 35000 rpm for 30 min, re-dispersed in water using an ultrasonic bath, washed with water, centrifuged again, and dialyzed to free them from unreacted materials.

Characterization

The AX sample used in this work was recharacterized according to the reported methods [34]. Elemental analysis

was carried out by CHNS analyzer (Vario MICRO V1.4.2; Elementar Analysensysteme, GmbH, Germany). Monosaccharide composition was determined by HPLC using Dionex ICS 3000 system, consisting of CarboPacPA20 column (0.4 × 150 mm) and electrochemical detector, according to a reported method [35] after acid hydrolysis [36]. ATR-FT-IR spectrum was recorded by Cary 630 FTIR Spectrometer (Agilent, USA). GPC was performed by Agilent 1200 series (Agilent, Germany) system using PL aquagel-OH mixed column (8 μm; 7.5 × 300 mm) and refractive index detector (G1362A). Water containing 0.1% $NaNO_3$ was used as eluent (flow rate, 1.0 mL min^{-1} at 70 °C) and injection volume was 10 μL. Data were analyzed by the ChemStation GPC Data Analysis Rev. A.02.02 (Agilent, Germany). Pullulan and dextran were used as calibration standards.

The AX-encapsulated ^{198}AuNPs samples were diluted four times with water, filtered through 0.22 μm membrane, and SPR spectra recorded on Pharmaspec UV-1700 spectrophotometer (Shimadzu, Japan) in 300–800 nm range using AX suspension as the reference. The SPR absorption at 526 nm was used to determine the particle size and concentration of Au was determined by using molar absorptivity value of 3.36×10^9 at 526 nm [37]. Stability of the particles was studied in human serum by recording SPR spectra 1 h, 2 h, 48 h, and 60 h after appropriate dilution with water.

The pXRD spectra of AX-encapsulated ^{198}AuNPs were recorded on Bruker D8 Discover (Germany) diffractometer using monochromatic Cu Kα radiation (λ = 1.5406 Å) operating at 40 kV and 30 mA. The data were collected over a 10–80° 2θ range. The size of particles was calculated from the highest intensity peak in the XRD spectra by use of Debye–Scherrer equation ($D = 0.9\lambda/\beta\cos\theta$) [38].

For transmission electron microscopy (TEM), an ultrasonically dispersed solution of the NPs was placed on a carbon-coated grid and images were obtained by JEM-1200EX (JEOL, Japan) microscope at an accelerating voltage of 120 kV.

Particle Size Distribution and Zeta Potential

Particle size and zeta potential were determined by NanoZS90 HPPS 5001 Zetasizer (Malvern, UK). The disposable cuvette was filled with the sample and allowed to equilibrate for 2–3 min at 21 °C before the measurement. Ten replicates of each sample were measured and an average value was reported.

For zeta potential (ζ) measurements, the capillary cell (DTS 1060) was flushed with water and filled with sample avoiding air bubbles in the capillary. Ten replicates were measured and the average values were reported.

Cell Viability and Cytotoxicity

Cytotoxicity of the AX-encapsulated ^{198}AuNPs was determined by neutral red (NR) [39] and potato disc assays [40]. Briefly, HeLa cells were cultured as monolayers into 96-well plate, containing approximately 1×10^4 cells in each well, DMEM culture medium supplemented with 10% of FBS, glucose (4.500 g L^{-1}), and 1% of penicillin-streptomycin. The plate was incubated at 37 °C for 24 h under 5% CO_2 and 90% humidity. To the cultured cells, three blanks (one excluding the AX and ^{198}AuNPs, the other containing AX (6.70 μg mL^{-1}) and excluding ^{198}AuNPs), third one excluding AX and containing ^{198}AuNP (18.0 μg mL^{-1}), and varying concentrations of AX-encapsulated^{198}AuNPs (18.0, 9.0, and 4.5 μg mL^{-1}) were added in 1:1 ratio and the plate was incubated again for 24 h under similar conditions. After incubation, the medium was drained, cells washed with PBS, the NR dye added, and the plate incubated for further 2 h. The surplus NR was washed out by freshly prepared de-staining solution (glacial acetic acid-ethanol-water, 1:49: 50) and the culture was incubated for further 10 min. The optical density of the released NR dye was measured at 570 nm. Relative cell viability was calculated as:

$$\text{Cell viability } (\%) = \frac{\text{sample absorbance}}{\text{control absorbance}} \times 100$$

The potato disc method was also used to assess the cytotoxicity of ^{198}AuNPs. For this, *A. tumefaciens* was grown on Luria broth medium for 48 h at 28 °C in shaking incubator. Various concentrations of ^{198}AuNPs (1.8, 9.0, and 4.5 μg mL^{-1}) and of AX suspension (67.0 μg mL^{-1} were tested. Inoculum was prepared by mixing each dilution (100 μL) with bacterial culture (100 μL). Negative control was prepared by mixing of water (100 μL) and *A. tumefaciens* (100 μL). Roxithromycin (100 ppm: 100 μL) was used as positive control. Red-skinned potatoes were purchased from a local market and surface sterilized by using 10% bleach solution. Cylinders of surface sterilized red-skinned potato were made with the help of sterilized borer. The 5-mm-thick discs of these potato cylinders were cut and placed on solidified agar plates (10 discs per plate). Inoculum (50 μL) was poured on the surface of each disc of respective concentration as well as controls. The discs were examined after 21 days of incubation under dissecting microscope after staining with Lugol's solution (potassium iodide-iodine-distilled water in 10:5:7 ratio). The number of tumors per disc was counted. The doses for the cytotoxicity tests were chosen by considering the radioactivity suitable for imaging.

Percentage inhibition for each concentration was determined by using the following formula.

$$\%\text{Inhibition} = \frac{\text{No. of tumors with sample}}{\text{No. of tumors with control}} \times 100$$

Biodistribution Studies

Biodistribution experiments were planned to be carried out in vivo after intravenous and oral administration to healthy rabbits, in tumor-bearing mouse, and in vitro among serum proteins as follows.

Biodistribution after Intravenous Administration of ^{198}AuNPs in Rabbit

These experiments were conducted at the Institute of Nuclear Medicine and Oncology hospital, Lahore. The AX suspension containing ^{198}AuNPs equivalent to 14.0 μg mL^{-1} Au having ~1000 μCi mL^{-1} activity was prepared by appropriately diluting the stock suspension. The dose (0.5 mL), adjusted to pH 7 by use of HCl (0.1 M) or NaOH (0.1 M) solutions, was filtered through 0.22-μm membrane (Polycarbonate, Sterlitech, USA) and injected into the ear vein of healthy rabbits ($n = 4$; local breed, age 12–16 weeks, average weight 900 ± 50 g). The animals were anesthetized by intramuscular ketamine injection (50 mg kg^{-1}) before administration of the dose. The administered dose was determined by subtracting the activity remaining in the syringe from the total taken in the syringe.

Whole body images of the animals were acquired in dynamic mode (for 15 min with 1 min interval) and at 5, 60, 120, 180 min, and 24 h post-injection by use of large field-of-view dual-head gamma camera (Infinia Hawkeye®, GE Healthcare, Milwaukee, USA) fitted with a high resolution and high energy collimator. The images were acquired from anterior, posterior, left lateral, right lateral, dorsal, and ventral views. After re-anesthetization at 180 min and 24 h post-injection, the animals were sacrificed and organs of interest and remaining carcass were collected, weighed, and counted for the radioactivity in a well-type Beckman 8000 gamma counter (Beckman, Brea, CA). Approximately 75% of the total blood volume was withdrawn by cardiac puncture and counted for radioactivity. The radioactivity in the sample and an aliquot of the injection mixture was determined and reported as percentage of injected dose per gram of the tissue.

Biodistribution after Oral Administration of ^{198}AuNPs in Rabbit

A suspension of AX-encapsulated ^{198}AuNPs containing 20.0 μg mL^{-1} Au having ~1200 μCi mL^{-1} activity in saline (2.00 mL) adjusted to pH 7 was administered orally to the rabbits ($n = 4$). The animals were anesthetized by intramuscular ketamine injection (50 mg kg^{-1}) and fixed on a wooden board. A flexible cannula was placed in the upper third of the esophagus and AX-encapsulated ^{198}AuNP suspension (2.0 mL) was gently instilled and images were recorded from anterior, posterior, left lateral, right lateral, dorsal, and ventral sides at 5 min, 0.5, 1, 2, 24, 48, and 96 h post-administration.

In Vitro Distribution of ^{198}AuNPs in Serum Proteins

Serum samples (0.5 mL, $n = 3$) from healthy human were vortex-mixed with equal volumes of AX-encapsulated ^{198}AuNPs equivalent to 14.0 μg mL^{-1} Au having ~ 1000 mCi mL^{-1} suspension and a buffer mixture (Tris, 2 SDS, 10% glycerol, and 0.0125% bromophenol blue; pH adjusted to 6.8 with HCl or NaOH solution). The samples were incubated at 37 °C for 1 h and subjected to SDS-polyacrylamide gel (SDS-PAGE) analysis at 50 mA/gel [41]. The gel was stained with a staining solution Coomassie brilliant blue R-250 in (water-methanol-glacial acetic acid, 50:10:0.25) for 10 min. The gel was de-stained in methanol-acetic acid-water solution

Table 1 Analytical data of AX, experimental (literature [34, 43] for FT-IR)

CHN (%)	C 31.61 (31.59), H 4.59 (4.66), N 1.05 (1.20)
Monosaccharides (%)	Ara 23.24 (23.11), Xyl 76.67 (76.89), uronic acids 1.3 (Not determined)
Protein (%)	Not detectable (not detectable)
Molar mass (g mol^{-1})	3.17×10^6 (3.26×10^6)
Moisture (%)	8.31 (8.24)
FT-IR bands (cm^{-1})	ν(OH) 3417 (3414), ν(CH) 2921 (2925), stretch due to absorbed water merged with carboxylic group 1634 (1630), in-plane δ(OH) 1457 (1462), δ(CH_2) 1423 (1417), δ(CH) 1367 (1375), antisym bridge oxygen δ 1257,1152 (1249, 1162), δ (CO) 1041 (1043), ν_{sym} (COC glycosidic linkage) 899 (896), polymer backbone vibrations 612, 531 (617,534)

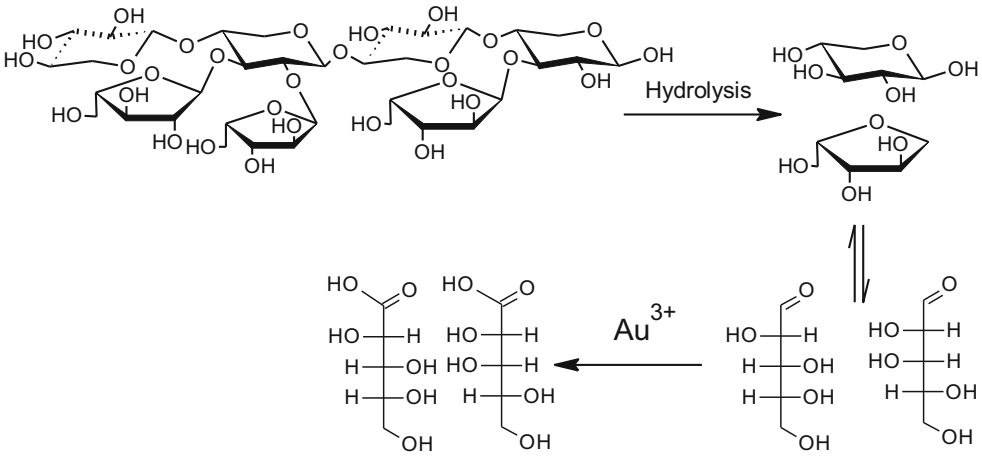

Scheme 1 AX undergoing partial hydrolysis followed by ring opening and oxidation by Au^{3+}

(250:100:650) until protein fractions appeared clear. The strips were dried for 2–3 min in air then at 70 °C in an oven for 30 min. The bands were cut (3×1 mm^2) and counted for radioactivity.

Hemocompatibility Study

Hemocompatibility of AX-encapsulated ^{198}AuNPs was studied by direct exposure for 3 h of fresh blood (0.5 mL) from healthy humans ($n = 4$) to ^{198}AuNPs (0.2 mL) equivalent to 14.0 μg mL^{-1} Au having ~ 1000 mCi mL-1 at 37 °C. Optical images were taken at 0, 5, 10, 30, 60, and 120 min by Euromex iScope (Holland) microscope; AX mucilage was used as the control.

Complement Activation

Complement fixation test was performed by turbidimetric method [42] by measuring the depletion of complement protein C_3 on incubation with the AX suspension and AX-encapsulated ^{198}AuNPs separately. The AX suspension (0.2 mL) and ^{198}AuNPs equivalent to 14.0 μg mL^{-1} of Au were incubated for 1 h at 37 °C with citrated blood

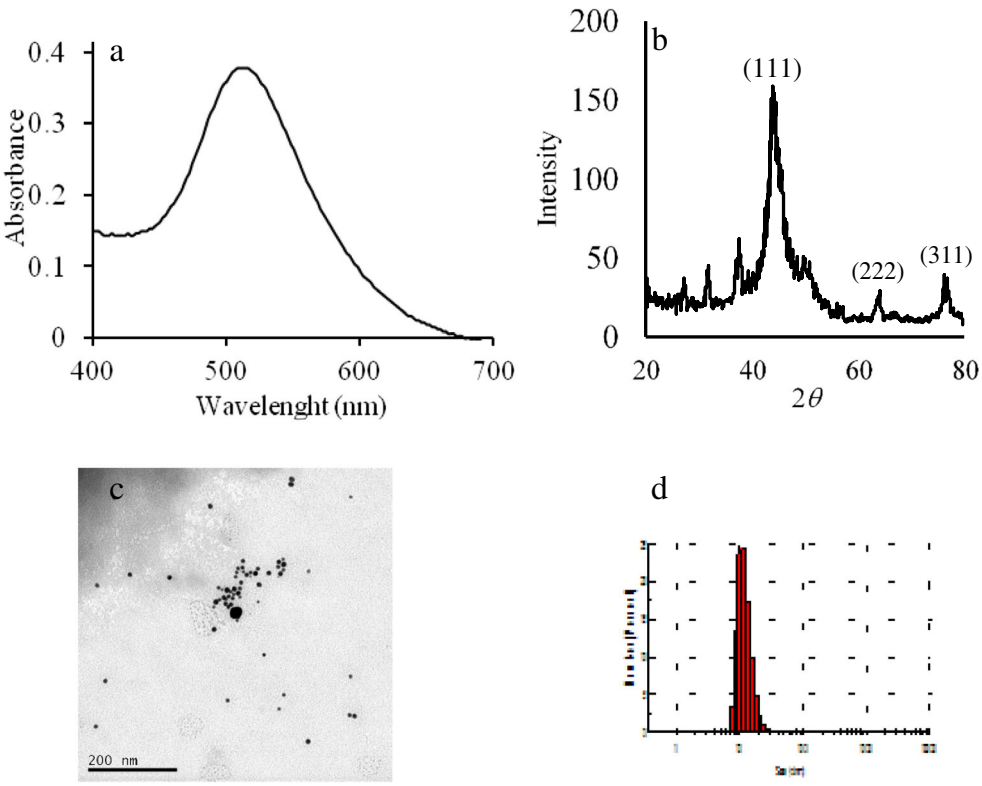

Fig. 1 Characterization of ^{198}AuNPs in AX (**a**), SPR spectrum (**b**), Powder XRD pattern of ^{198}AuNPs (**c**), and TEM images (**d**). Histogram of size distribution ^{198}AuNPs measured by DLS technique

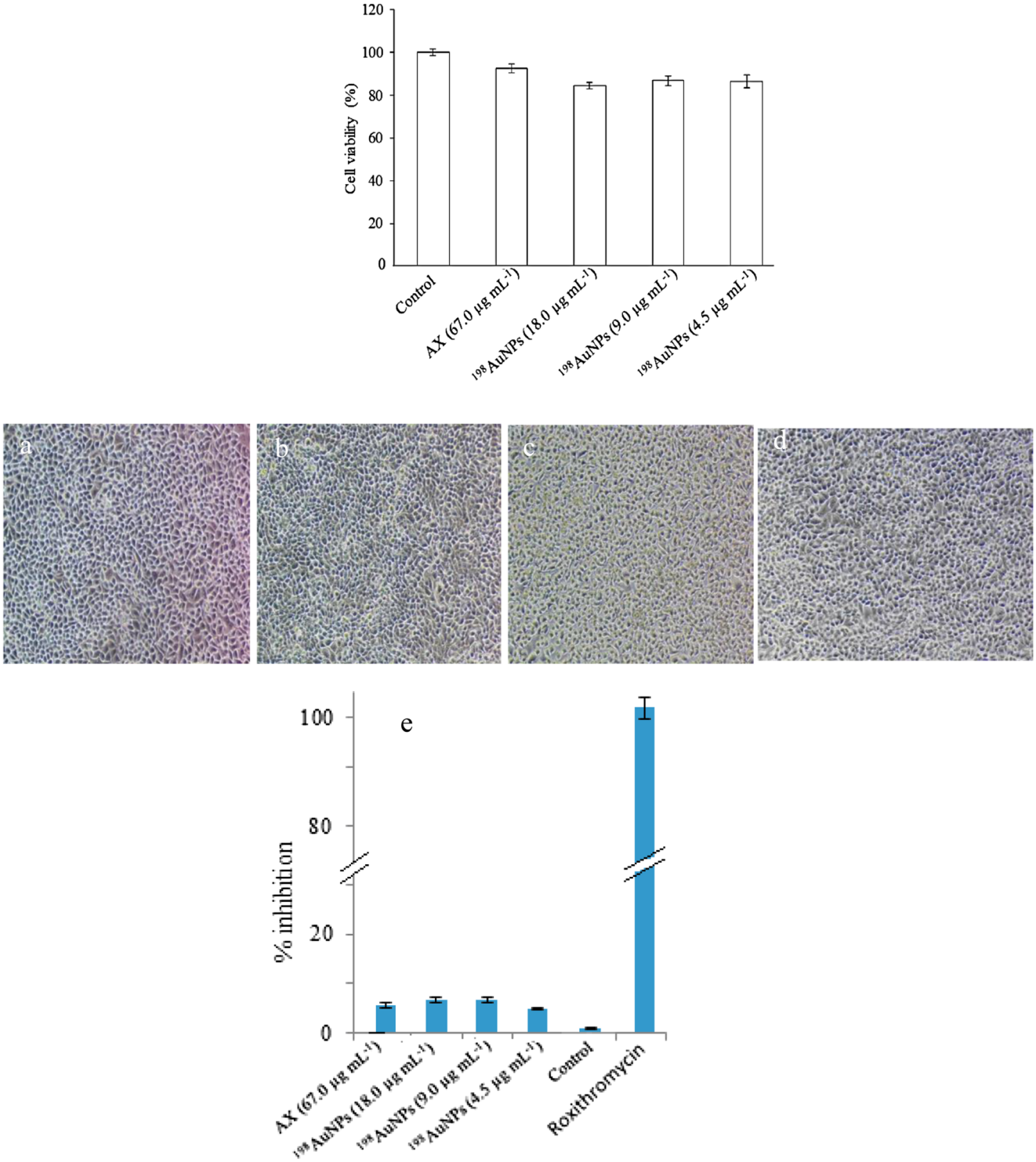

Fig. 2 Top: Histogram showing percentage of cell viability against HeLa cell line after incubation with AX suspension; bottom: (**a**) microscopic images of the control cells, (**b**) AX-treated cells, (**c**) AX-encapsulated ^{198}AuNP-treated cells, (**d**) ^{198}AuNP-treated cells showing no morphological changes, and (**e**) histogram showing percentage of inhibition of *A. tumefaciens* by AX-encapsulated ^{198}AuNPs and roxithromycin used as positive control in potato disc assay. The results are expressed as the mean ± SD ($n = 6$, $p < 0.05$, the error bars represent SD)

(0.2 mL). The final concentration of the ^{198}AuNPs in the assay was adjusted to 7.0 μg mL^{-1}. The assay was performed in triplicate according to the protocol provided by the kit manufacturer.

Statistical Analysis

The data were analyzed by employing the Student *t* test and one way-ANOVA where appropriate using Statgraphics® Centurion 18 (Statgraphics Technologies, Inc., USA) software with $p < 0.05$ significance level. The graphs were plotted by use of MS Excel® 2010.

Results and Discussion

AX from ispaghula is a well-established food ingredient and herbal remedy for bowel disorders. It is a well-characterized highly branched hemicellulosic material soluble in alkaline and insoluble in acidic media [43]. The AX used in the present work was found to be similar to the previously reported material [34] as revealed by elemental, monosaccharide, ATR-FT-IR, and GPC analyses (Table 1). Other than ispaghula, AX is found in a variety of cereal grains including rice, wheat, corn, rye, oat, barley, and sorghum. It is also part of several plant cell walls such as bamboo and pangola grass [44]. It has a linear Xyl*p* backbone, partially substituted with α-L-Ara*f* residues on O-3 or O-2 or both of the Xyl*p* units (Scheme 1) [45]. It is composed of arabinose and xylose which are reducing sugars. The monosaccharides are released on partial hydrolysis of the polysaccharide in acidic environment provided by the gold salt, $H^{198}AuCl_4 \cdot 3H_2O$, in the present work. The cyclic structure of the monosaccharides is known to exist in equilibrium with the aldose form that affords reduction of Au^{3+} to Au^0 in the reaction mixture. This process is outlined in Scheme 1.

Our previous experience with AX for synthesis of non-radioactive AuNPs [29] prompted us to use this material for synthesis of ^{198}AuNPs. Among 36 radioisotopes of gold, ^{198}Au is the most common isotope used for diagnosis and radiotherapy due to its appropriate half-life of 2.7 days [22]. Therefore, we attempted to synthesize ^{198}AuNPs using AX as reducing and capping agent for diagnostic imaging.

Synthesis and Characterization of ^{198}AuNPs

The ^{198}AuNPs were successfully prepared according to the method described in the "Materials and Methods" section. It was observed that AX reduced gold ions to NPs within 25 min at 50 °C. The optimal time and temperature were determined through preliminary experiments. The reduction process was witnessed by color changes from yellow to purple and finally to ruby red. The reaction was monitored by recording the SPR spectra in the 350–800 nm range (Fig. 1a). The position of the absorption band at 526 nm indicates that the particles are spherical in shape having an average size of 30 nm [37]. The optimum conditions to obtain the SPR band at 526 nm were: amount of mucilage (0.1%) 16 mL/40 mL, amount of $H^{198}AuCl_4$ (0.1 mM) 20 mL/40 mL, pH 8, time 25 min, and temperature 50 °C.

The XRD spectra (Fig. 1b) revealed characteristic face-centered cubic phase (JCPDS File No. 87-0720). The peaks were assigned to (1 1 1), (2 0 0), (2 2 2), and (3 1 1) planes of the nanocrystalloids. The intensities of the peaks suggest that the NPs were mainly oriented along (1 1 1) plane. The average size ($n = 3$) of the particles calculated from the XRD spectra by use of Debye–Scherrer equation was found to be 28 ± 3 nm. The TEM image (Fig. 1c) revealed that the particles were spherical in shape with size range of 25–30 nm. The DLS analysis provides information about hydrodynamic diameter and polydispersity index (PDI) of NPs. The hydrodynamic diameter thus determined was 101.4 ± 1.2 at pH 8. The relatively larger diameter by DLS indicates that the particles were covered with the AX film which swells on contact with the buffer solution [46]. The ζ value -23.5 ± 3.2 indicated that the

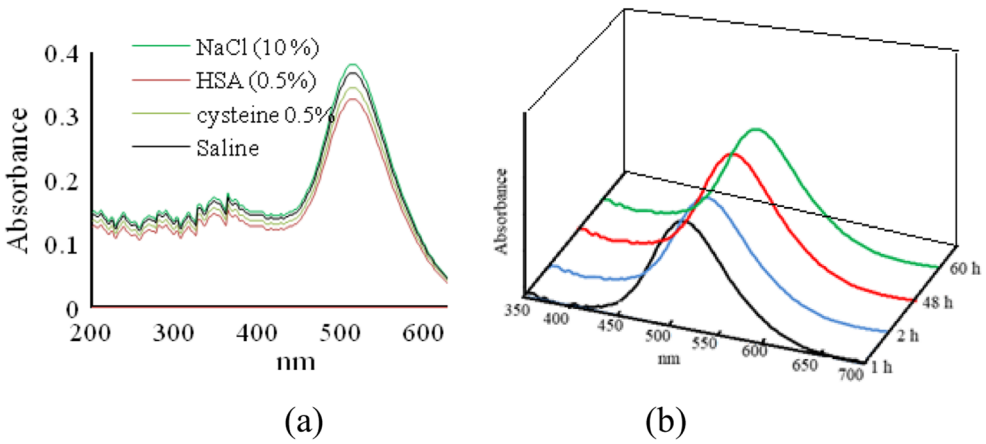

Fig. 3 (**a**) Spectra showing stability (absence of 320-nm band) of AX-encapsulated ^{198}AuNPs in different media. (**b**) The SPR spectra of AX-encapsulated ^{198}AuNPs in 0.2 M HSA showing no significant shift in wavelength and absorbance with time

particles should be stable for a couple of months [47]. However, the particles synthesized by use of AX in the present work exhibited exceptional stability extending over 3 years, which suggests that the AX plays a role in imparting exceptional stability to the particles. The PDI value of 0.322 reveals a narrow size distribution (Fig. 1d).

Cell Viability and Cytotoxicity Study

Biocompatibility of the AX-encapsulated ^{198}AuNPs was assessed by the NR uptake assay that provided a quantitative estimation of the number of viable cells in the culture. It is one of the widely used tests for the purpose [39]. It

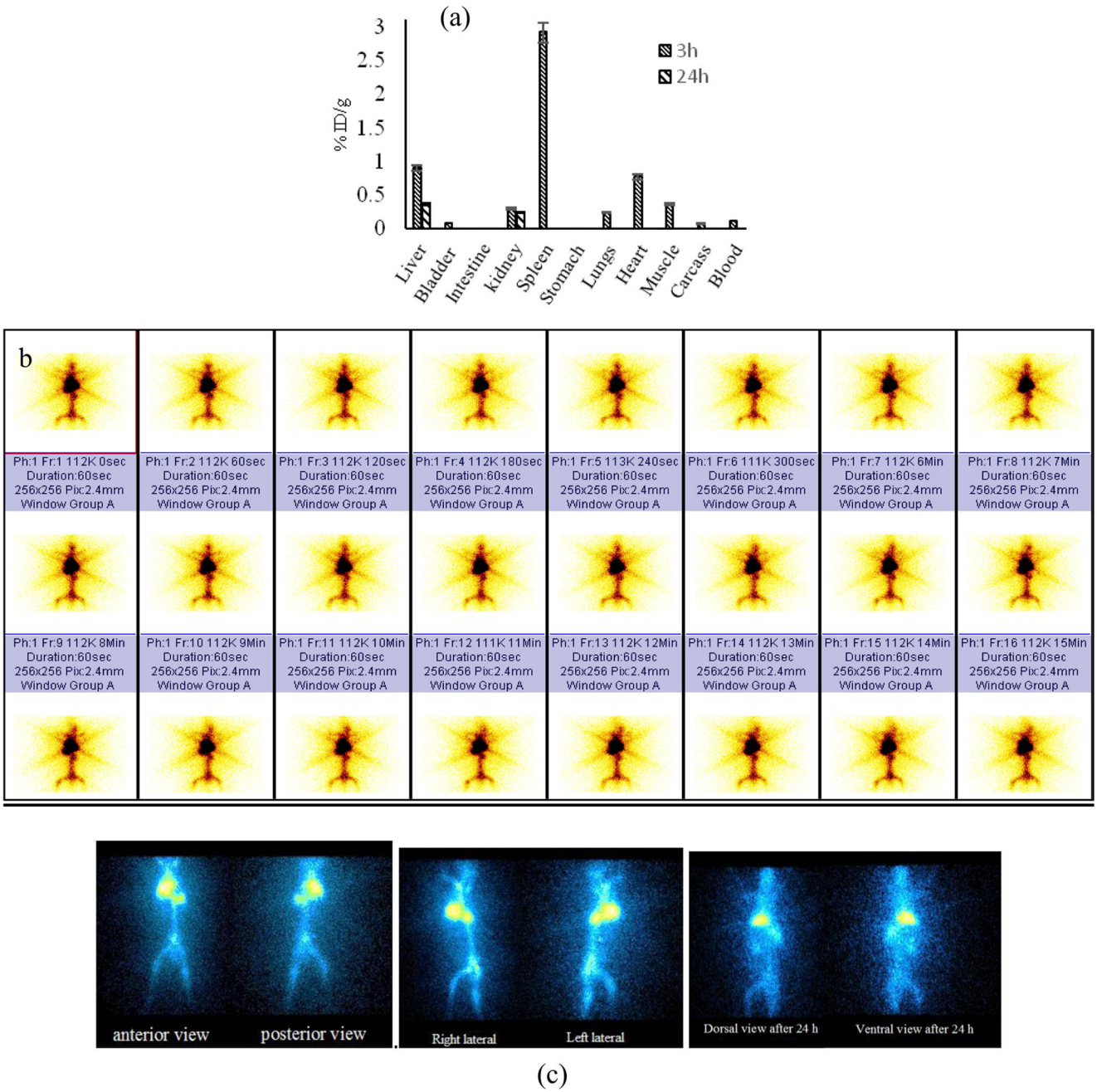

Fig. 4 (**a**) Biodistribution of ^{198}AuNPs (equivalent to 14.0 μg mL^{-1} Au, activity ~ 1000 μCi mL^{-1}. The rabbits were anesthetized by 50 mg kg^{-1} intramuscular ketamine injection) before administration of the dose) in various organs at 3 h and 24 h after i.v. administration; the amount of gold is expressed as a percentage of injected dose per gram (% ID g^{-1}) of organ/tissue. The results are expressed as the mean ± SD ($n = 4$, $p < 0.05$, the error bars represent SD). (**b**) Dynamic gamma camera images up to 15 min post i.v. injection (pH 7; 14.0 μg mL^{-1}; 1000 μCi mL^{-1}). (**c**) Gamma camera images of whole body (anterior, posterior, right lateral, and left lateral views) at 180 min post-injection, dorsal at 24 h, and ventral at 24 h, showing accumulation of radioactivity in the liver and spleen, with negligible amount in other organs

was found that incubation of HeLa cells with AX, AX-encapsulated ^{198}AuNPs at different concentrations, and ^{198}AuNPs did not affect the viability and morphology of the cells significantly (Fig. 2a–d) indicating their non-toxic nature. Thus, the AX-encapsulated ^{198}AuNPs can be used for in vivo diagnostic studies.

In order to rule out the interference of ^{198}AuNPs with neutral red assay, a secondary cytotoxicity test was performed by potato disc assay. In this assay, the tumor was induced by *A. tumefaciens*, which is considered histologically similar to that in animals and humans [40, 48]. A negligible inhibition, i.e., < 5%, was observed (Fig. 2e) suggesting the non-toxic nature of particles.

Biodistribution after Intravenous Administration of ^{198}AuNPs in Rabbit

In order to validate the in vivo study, stability of the AX-encapsulated ^{198}AuNPs was checked in vitro in biologically relevant media [49] including 10% NaCl, 0.2 M cysteine, 0.2 M histidine, and 0.2 M HSA at physiological pH for the time required to complete the study, i.e., 60 h. Typical spectra in HSA on time scale are shown in Fig. 3b. The AX-encapsulated ^{198}AuNP suspensions were found to be stable in all these media for that time. It was observed that there was no appearance of the band around 320 nm, characteristic of Au^{3+} compounds [50]. This clearly suggests that the particles do not ionize in the period under investigation.

Biodistribution data and gamma camera images obtained after i.v. administration of AX-encapsulated ^{198}AuNPs at fixed intervals of time are exhibited in Fig. 4. Highest uptake of ^{198}AuNPs after 3 h was found in the spleen followed by liver, heart, muscle, kidneys, and lungs (Fig. 4a). After 24 h, the activity was not detectable in the spleen and was significantly higher in the liver.

Biodistribution after Oral Administration of ^{198}AuNPs in Rabbit

The gamma camera images obtained after oral administration of AX-encapsulated ^{198}AuNPs are shown in Fig. 5. It can be seen that the activity did not move from the stomach even after 24 h. This means that the particles are firmly encapsulated by AX, which coagulated there being insoluble in acidic medium. This effect was verified when the activity moved on oral administration of 1% sodium bicarbonate solution (5 mL) and accumulated in the colon and remained confined there up to the last observation at 96 h. These results suggest that the AX-encapsulated ^{198}AuNPs may be used for a drug delivery at the colon or as diagnostic probes. At the colon, there is a host of enzymes including glycosidases and xylosidases, which would hydrolyze AX [51] in addition to a basic pH there.

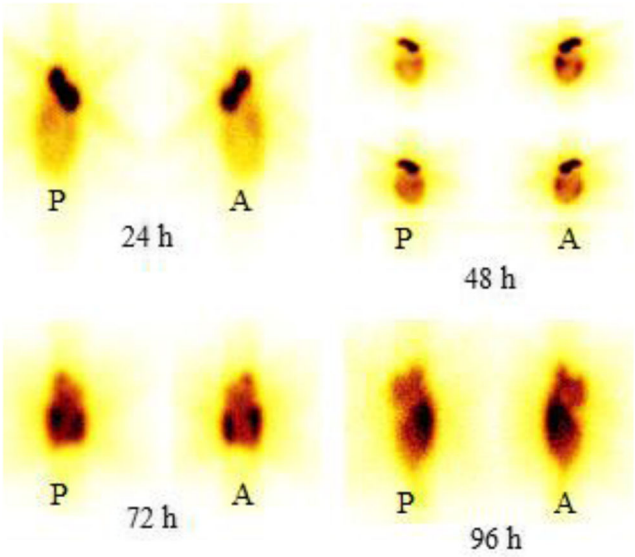

Fig. 5 Gamma camera images exhibiting accumulation of radioactivity at colon after oral administration of AX ^{198}AuNP (equivalent to 20.0 μg mL^{-1} Au, activity ~ 1200 μCi mL^{-1} in 2.0 mL saline adjusted to pH 7. The animals ($n = 4$) were anesthetized by 50 mg kg^{-1} intramuscular ketamine injection before administration) to rabbit in colon after 24, 48, 72, and 96 h. A, anterior; P, posterior

Thus, this study presents AX as a highly biocompatible capping agent for AuNPs for their use in medicine. A problem associated with other colon-specific drug delivery systems [52] is that a major drug loss occurs before they reach the ileocecal junction.

In Vitro Distribution of ^{198}AuNPs in Serum Proteins

Five protein bands separated after incubation of healthy human serum with AX-encapsulated ^{198}AuNPs are shown in Fig. 6 and distribution of radioactivity in these bands is

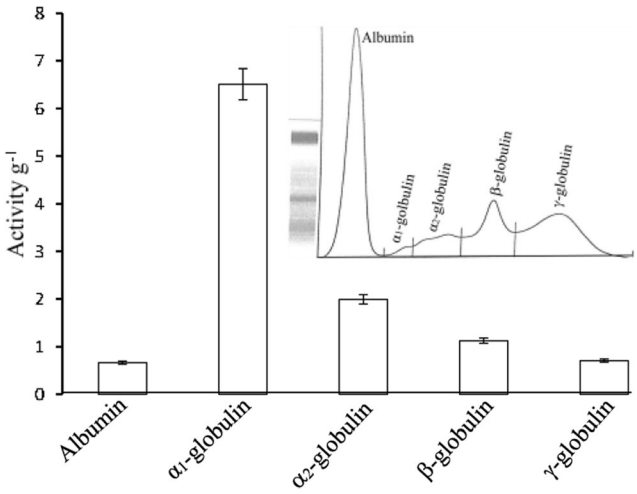

Fig. 6 In vitro distribution of AX-encapsulated ^{198}AuNPs (equivalent to 14.0 μg mL^{-1} Au, activity ~ 1000 mCi mL^{-1}) in serum proteins SDS-PAGE analysis; the results are expressed as the mean ± SD ($n = 4$, $p < 0.05$, error bars represent SD). Inset shows separated protein bands

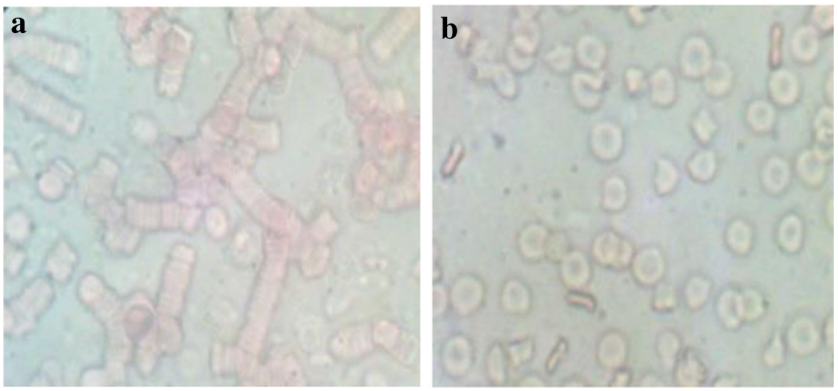

Fig. 7 Optical images exhibiting rouleaux effect (**a**) AX-treated cells and (**b**) no effect by AX-encapsulated ^{198}AuNPs (200 μCi:500 μL) after 120 min

depicted as bar graph (Fig. 6). The highest affinity of gold was recorded for α_1-globulin (6.5%) followed by α_2-globulin (~ 2%), β-globulin (~ 1%), γ-globulin (0.707%), and albumin (0.66%). Binding of gold with globulins from auranofin, an oral gold drug for rheumatoid arthritis, has also been reported previously [53, 54]. These results suggest that globulins can be labeled with radioactive gold by use of AX-encapsulated ^{198}AuNPs. Globulins play important role in inflammatory and malignancy processes. Therefore, the ^{198}Au-labeled globulins may find some useful applications as diagnostics and therapeutics.

Hemocompatibility Study

This study was carried out to assess the morphological effects of AX-encapsulated ^{198}AuNPs on blood cells. No hemolysis was observed, whereas rouleaux effect (Fig. 7) was there with AX without NPs. The rouleaux effect is commonly observed with polysaccharides and polyols [55] and is not a deleterious effect. Mechanism of such type of aggregation of erythrocytes is not yet fully understood.

Complement Activation

The amount of C_3 in blood before incubation was 128%. After incubation with AX and ^{198}AuNPs separately, the amount of C_3 was 125 ± 6.35% and 129 ± 5.14%, respectively. These results clearly indicate that AX and ^{198}AuNPs do not activate the complement system. Thus, the AX-encapsulated ^{198}AuNPs appear to be biocompatible [50].

Conclusions

This study demonstrates that ^{198}AuNPs synthesized by use of AX (a food material) as the reducing and dispersing agent are non-toxic to HeLa cells and *A. tumefaciens* and biocompatible. The AX-encapsulated ^{198}AuNPs exhibited different biodistribution in vivo depending upon the route of administration. After oral administration, they accumulated at the colon in rabbit after passing through the stomach and produced good-quality gamma images. After i. v. administration to rabbit and mouse, they accumulated in the liver. Thus, the AX-encapsulated ^{198}AuNPs appear to have potential for use as diagnostic and therapeutic agents. Since ^{198}Au is both γ and β emitter, these particles show a promise for use in image-guided nanoparticle therapies of cancer and advanced drug delivery devices. In diagnostics, gamma imaging is preferred because of its lower limit of detection as compared to other techniques. These properties have been imparted to the particles by the presence of AX.

Compliance with Ethical Standards

Conflict of Interest The authors declare that they have no conflict of interest.

Ethical Approval for Use of Human Blood and Animals The study protocols regarding use of human blood and animals were reviewed and approved by the Institutional Review Board of Forman Christian College Lahore. Written informed consent was obtained from the blood donors (healthy human adults). Guidelines provided in Good Clinical Practice by ICH, World Medical Association Declaration of Helsinki and APA Committee on Animal Research and Ethics (CARE), USA, were followed.

References

1. Riley RS, Day ES (2017) Gold nanoparticle-mediated photothermal therapy: applications and opportunities for multimodal cancer treatment. Wiley Interdiscip Rev Nanomed Nanobiotech 9
2. Mahan MM, Doiron AL (2018) Gold nanoparticles as X-ray, CT, and multimodal imaging contrast agents: formulation, targeting, and methodology. J Nanomater 2018:1–15
3. Ruan S, Yuan M, Zhang L et al (2015) Tumor microenvironment sensitive doxorubicin delivery and release to glioma using angiopep-2 decorated gold nanoparticles. Biomaterials 37:425–435. https://doi.org/10.1016/j.biomaterials.2014.10.007
4. Manohar N, Reynoso FJ, Diagaradjane P, Krishnan S, Cho SH (2016) Quantitative imaging of gold nanoparticle distribution in a tumor-bearing mouse using benchtop x-ray fluorescence computed tomography. Sci Rep 6:22079. https://doi.org/10.1038/srep22079

5. Vigderman L, Zubarev ER (2013) Therapeutic platforms based on gold nanoparticles and their covalent conjugates with drug molecules. Adv Drug Deliv Rev 65:663–676. https://doi.org/10.1016/j.addr.2012.05.004
6. Jain PK (2014) Gold nanoparticles for physics, chemistry and biology. Edited by Catherine Louis and Olivier Pluchery. Angew Chem Int Ed 53:1197–1197. https://doi.org/10.1002/anie.201309807
7. Nam J-M, Thaxton CS, Mirkin CA et al (2009) Gold nanoparticles: assembly, supramolecular chemistry, quantum-size-related properties, and applications toward biology, catalysis, and nanotechnology. Nature 9:1–8. https://doi.org/10.1016/j.toxlet.2005.10.003
8. Her S, Jaffray DA, Allen C (2017) Gold nanoparticles for applications in cancer radiotherapy: mechanisms and recent advancements. Adv Drug Deliv Rev 109:84–101
9. Austin LA, MacKey MA, Dreaden EC, El-Sayed MA (2014) The optical, photothermal, and facile surface chemical properties of gold and silver nanoparticles in biodiagnostics, therapy, and drug delivery. Arch Toxicol 88:1391–1417
10. Qu X, Li Y, Li L, et al (2015) Fluorescent gold nanoclusters: synthesis and recent biological application. J Nanomater 2015:Article ID 784097
11. Ma Z, Xia H, Liu Y, Liu B, Chen W, Zhao YD (2013) Applications of gold nanorods in biomedical imaging and related fields. Chin Sci Bull 58:2530–2536. https://doi.org/10.1007/s11434-013-5720-7
12. Jain PK, Lee KS, El-Sayed IH, El-Sayed MA (2006) Calculated absorption and scattering properties of gold nanoparticles of different size, shape, and composition: applications in biological imaging and biomedicine. J Phys Chem B 110:7238–7248. https://doi.org/10.1021/jp057170o
13. Liu X, Atwater M, Wang J, Huo Q (2007) Extinction coefficient of gold nanoparticles with different sizes and different capping ligands. Colloids Surf B: Biointerfaces 58:3–7. https://doi.org/10.1016/j.colsurfb.2006.08.005
14. Alric C, Taleb J, Le Duc G et al (2008) Contrast agents for both X-ray computed tomography and magnetic resonance imaging. J Am Chem Soc 130:5908–5915. https://doi.org/10.1021/ja078176p
15. Norouzi H, Khoshgard K, Akbarzadeh F (2018) In vitro outlook of gold nanoparticles in photo-thermal therapy: a literature review. Lasers Med Sci 33:917–926
16. Huang X, El-Sayed MA (2011) Plasmonic photo-thermal therapy (PPTT). Alexandria J Med 47:1–9. https://doi.org/10.1016/j.ajme.2011.01.001
17. Axiak-Bechtel SM, Upendran A, Lattimer JC, Kelsey J, Cutler CS, Selting KA, Bryan JN, Henry CJ, Boote E, Tate DJ, Bryan ME, Katti KV, Kannan R (2014) Gum arabic-coated radioactive gold nanoparticles cause no short-term local or systemic toxicity in the clinically relevant canine model of prostate cancer. Int J Nanomedicine 9:5001–5011. https://doi.org/10.2147/IJN.S67333
18. Shukla R, Chanda N, Zambre A, Upendran A, Katti K, Kulkarni RR, Nune SK, Casteel SW, Smith CJ, Vimal J, Boote E, Robertson JD, Kan P, Engelbrecht H, Watkinson LD, Carmack TL, Lever JR, Cutler CS, Caldwell C, Kannan R, Katti KV (2012) Laminin receptor specific therapeutic gold nanoparticles (198AuNP-EGCg) show efficacy in treating prostate cancer. Proc Natl Acad Sci 109:12426–12431. https://doi.org/10.1073/pnas.1121174109
19. Chanda N, Kan P, Watkinson LD, Shukla R, Zambre A, Carmack TL, Engelbrecht H, Lever JR, Katti K, Fent GM, Casteel SW, Smith CJ, Miller WH, Jurisson S, Boote E, Robertson JD, Cutler C, Dobrovolskaia M, Kannan R, Katti KV (2010) Radioactive gold nanoparticles in cancer therapy: therapeutic efficacy studies of GA-198AuNP nanoconstruct in prostate tumor-bearing mice. Nanomedicine 6:201–209. https://doi.org/10.1016/j.nano.2009.11.001
20. Radionuclide NR, Phillips WT, Otto RA, Bao A (2011) Interventional therapy of head and neck cancer with lipid nanoparticle-carried Rhenium-186 radionuclide. J Vasc Interv Radiol 21:1271–1279. https://doi.org/10.1016/j.jvir.2010.02.027. Interventional
21. Al-Yasiri AY, Khoobchandani M, Cutler CS et al (2017) Mangiferin functionalized radioactive gold nanoparticles (MGF- 198 AuNPs) in prostate tumor therapy: green nanotechnology for production, in vivo tumor retention and evaluation of therapeutic efficacy. Dalton Trans 46:14561–14571. https://doi.org/10.1039/C7DT00383H
22. Tobias JS, Hochhauser D (2009) Cancer and its management. Wiley, Hoboken
23. Kim D, Park S, Jae HL et al (2007) Antibiofouling polymer-coated gold nanoparticles as a contrast agent for in vivo X-ray computed tomography imaging. J Am Chem Soc 129:7661–7665. https://doi.org/10.1021/ja071471p
24. Lee J, Chatterjee DK, Lee MH, Krishnan S (2014) Gold nanoparticles in breast cancer treatment: promise and potential pitfalls. Cancer Lett 347:46–53
25. Hainfeld JF, Slatkin DN, Smilowitz HM (2004) The use of gold nanoparticles to enhance radiotherapy in mice. Phys Med Biol:49. https://doi.org/10.1088/0031-9155/49/18/N03
26. Chen Y, Wang X (2008) Novel phase-transfer preparation of monodisperse silver and gold nanoparticles at room temperature. Mater Lett 62:2215–2218. https://doi.org/10.1016/j.matlet.2007.11.050
27. Jeong GH, Lee YW, Kim M, Han SW (2009) High-yield synthesis of multi-branched gold nanoparticles and their surface-enhanced Raman scattering properties. J Colloid Interface Sci 329:97–102. https://doi.org/10.1016/J.JCIS.2008.10.004
28. Deraedt C, Salmon L, Gatard S, Ciganda R, Hernandez R, Ruiz J, Astruc D (2014) Sodium borohydride stabilizes very active gold nanoparticle catalysts. Chem Commun 50:14194–14196. https://doi.org/10.1039/c4cc05946h
29. Amin M, Iram F, Iqbal MS, Saeed MZ, Raza M, Alam S (2013) Arabinoxylan-mediated synthesis of gold and silver nanoparticles having exceptional high stability. Carbohydr Polym 92:1896–1900. https://doi.org/10.1016/j.carbpol.2012.11.056
30. Iram F, Iqbal MS, Athar MM, Saeed MZ, Yasmeen A, Ahmad R (2014) Glucoxylan-mediated green synthesis of gold and silver nanoparticles and their phyto-toxicity study. Carbohydr Polym 104:29–33. https://doi.org/10.1016/j.carbpol.2014.01.002
31. Rabito MF, Reis AV, dos Reis Freitas A et al (2012) A pH/enzyme-responsive polymer film consisting of Eudragit® FS 30 D and arabinoxylane as a potential material formulation for colon-specific drug delivery system. Pharm Dev Technol 17:429–436. https://doi.org/10.3109/10837450.2010.546409
32. Agarwal VK, Gupta A, Chaturvedi S, Khan F (2016) Polysaccharide: carrier in colon targeted drug delivery system. MIT Int J Pharm Sci 2:1–9
33. Lemarchand C, Gref R, Couvreur P (2004) Polysaccharide-decorated nanoparticles. Eur J Pharm Biopharm 58:327–341
34. Massey S, Iqbal MS, Wolf B et al (2016) Comparative drug loading and release study on some carbohydrate polymers. Lat Am J Pharm 35:146–155
35. Weitzhandler M, Barreto V, Pohl C, Jandik P, Cheng J, Avdalovic N (2004) CarboPacTM PA20: a new monosaccharide separator column with electrochemical detection with disposable gold electrodes. J Biochem Biophys Methods 60:309–317. https://doi.org/10.1016/j.jbbm.2004.01.009
36. Saeman JF, Moore WE, Mitchell RL, Millett MA (1954) Techniques for the determination of pulp constituents by quantitative paper chromatography. TAPPI J 37:336–343
37. Rahman S (2016) Size and concentration analysis of gold nanoparticles with ultraviolet-visible spectroscopy. Undergrad J Math Model One + Two 7:13. https://doi.org/10.5038/2326-3652.7.1.4872
38. Scherrer P (1918) Bestimmung der Größe und der inneren Struktur von Kolloidteilchen mittels Röntgenstrahlen. Nachrichten von der

Gesellschaft der Wissenschaften zu Göttingen, Math Klasse 1918: 98–100
39. Repetto G, del Peso A, Zurita JL (2008) Neutral red uptake assay for the estimation of cell viability/cytotoxicity. Nat Protoc 3:1125–1131. https://doi.org/10.1038/nprot.2008.75
40. Trigui F, Pigeon P, Jalleli K et al (2013) Selection of a suitable disc bioassay for the screening of anti-tumor molecules. Int J Biomed Sci 9:230–236
41. Laemmli UK (1970) Cleavage of structural proteins during the assembly of the head of bacteriophage T4. Nature 227:680–685
42. Parker AR, Jolles S, Ponsford M et al (2018) Quantification of human C1 esterase inhibitor protein using an automated turbidimetric immunoassay. J Clin Lab Anal 33:e22627. https://doi.org/10.1002/jcla.22627
43. Saghir S, Iqbal MS, Hussain MA, Koschella A, Heinze T (2008) Structure characterization and carboxymethylation of arabinoxylan isolated from Ispaghula (Plantago ovata) seed husk. Carbohydr Polym 74:309–317. https://doi.org/10.1016/j.carbpol.2008.02.019
44. Izydorczyk MS, Biliaderis CG, Lazaridou A et al (2007) Functional food carbohydrates. CRC Press, Boca Raton
45. Iram F, Massey S, Iqbal MS, Ward DG (2018) Structural investigation of hemicelluloses from *Plantago ovata*, *Mimosa pudica* and Lallemantia royleana by MALDI-ToF mass spectrometry. J Carbohydr Chem 37:1–17. https://doi.org/10.1080/07328303.2018.1487973
46. Tomaszewska E, Soliwoda K, Kadziola K, et al (2013) Detection limits of DLS and UV-Vis spectroscopy in characterization of polydisperse nanoparticles colloids. J Nanomater 2013:60. https://doi.org/10.1155/2013/313081
47. Bhattacharjee S (2016) DLS and zeta potential - what they are and what they are not? J Control Release 235:337–351
48. Smith EF (1916) Studies on the crown gall of plants its relation to human cancer. J Cancer Res 1:231–309. https://doi.org/10.1158/jcr.1916.231
49. Kattumuri V, Katti K, Bhaskaran S, Boote EJ, Casteel SW, Fent GM, Robertson DJ, Chandrasekhar M, Kannan R, Katti KV (2007) Gum arabic as a phytochemical construct for the stabilization of gold nanoparticles: in vivo pharmacokinetics and X-ray-contrast-imaging studies. Small 3:333–341. https://doi.org/10.1002/smll.200600427
50. Brown DH, McKinlay GC, Smith WE (1979) The electronic spectra of some gold(III) complexes. Inorg Chim Acta 32:117–121. https://doi.org/10.1016/S0020-1693(00)91648-7
51. Swarbrick J (1996) Encyclopedia of pharmaceutical technology. Pharm Technol 3:2004–2020. https://doi.org/10.1081/E-EPT-100001065
52. Philip A, Philip B (2010) Colon targeted drug delivery systems: a review on primary and novel approaches. Oman Med J 25:70–78. https://doi.org/10.5001/omj.2010.24
53. Iqbal MS, Taqi SG, Arif M, Wasim M, Sher M (2009) In vitro distribution of gold in serum proteins after incubation of sodium aurothiomalate and auranofin with human blood and its pharmacological significance. Biol Trace Elem Res 130:204–209. https://doi.org/10.1007/s12011-009-8330-0
54. Israel L, Edelstein R, Mannoni P, Radot E, Greenspan EM (1977) Plasmapheresis in patients with disseminated cancer: clinical results and correlation with changes in serum protein. The concept of "nonspecific blocking factors.". Cancer 40:3146–3154. https://doi.org/10.1002/1097-0142(197712)40:6<3146::AID-CNCR2820400659>3.0.CO;2-N
55. Robyt JF (1998) Essentials of carbohydrate chemistry. Springer Science & Business Media, Berlin